



Contents lists available at SciVerse ScienceDirect

Earth and Planetary Science Letters

journal homepage: www.elsevier.com/locate/epsl

Coupled high-resolution marine and terrestrial records of carbon and hydrologic cycles variations during the Paleocene–Eocene Thermal Maximum (PETM)

Brett J. Tipple^{a,*}, Mark Pagani^a, Srinath Krishnan^a, Sitindra S. Dirghangi^a, Simone Galeotti^b, Claudia Agnini^c, Luca Giusberti^c, Domenico Rio^c

^a Yale University, Department of Geology and Geophysics, P.O. Box 208109, New Haven, CT, 06520-8109, United States

^b Istituto di Geologia, Università di Urbino, Urbino, Pesaro and Urbino, Italy

^c Dipartimento di Geoscienze, Università degli Studi di Padova, Padova, Italy

ARTICLE INFO

Article history:

Received 17 January 2011

Received in revised form 1 July 2011

Accepted 30 August 2011

Available online xxxx

Editor: P. DeMenocal

Keywords:

carbon isotopes
hydrogen isotopes
leaf waxes
n-alkanes
PETM

ABSTRACT

The Paleocene–Eocene Thermal Maximum is characterized by a massive perturbation of the global carbon cycle reflected in a large, negative carbon isotope excursion associated with rapid global warming and changes in the hydrologic system. The magnitude of the carbon isotope excursion from terrestrial carbonates and organic carbon is generally larger relative to marine carbonates. However, high-resolution marine and terrestrial isotopic records from the same locality for direct comparison are limited. Here we present coupled carbon isotope records from terrestrial biomarkers ($\delta^{13}\text{C}_{n\text{-alkane}}$), marine bulk carbonates ($\delta^{13}\text{C}_{\text{carbonate}}$), and bulk organic carbon ($\delta^{13}\text{C}_{\text{organic}}$) from the continuous sedimentary record of the Forada section in northern Italy in order to evaluate the magnitude and phase relationships between terrestrial and marine environments. Consistent with previous reports, we find that the carbon isotope excursion established from $\delta^{13}\text{C}_{n\text{-alkane}}$ values is more negative than those established from $\delta^{13}\text{C}_{\text{carbonate}}$ and $\delta^{13}\text{C}_{\text{organic}}$ values. In contrast to the majority of PETM records, all Forada $\delta^{13}\text{C}$ records show a sharp ^{13}C -enrichment immediately following the onset of the carbon isotope excursion. Further, the terrestrial $\delta^{13}\text{C}_{n\text{-alkane}}$ record lags $\delta^{13}\text{C}_{\text{carbonate}}/\delta^{13}\text{C}_{\text{organic}}$ trends by ~4–5 kyr—offsets that reflect the long residence time of soil organic carbon.

Hydrogen isotope records from higher-plant leaf waxes ($\delta\text{D}_{n\text{-alkane}}$) and sea-surface temperatures (TEX_{86}) were established to assess hydrologic and ocean temperature trends. We find $\delta\text{D}_{n\text{-alkane}}$ values trend more positive, associated with higher temperatures prior to the onset of the carbon isotope excursion, and conclude that regional changes in the hydrologic cycle likely occurred before the onset of the carbon isotope anomaly.

© 2011 Elsevier B.V. All rights reserved.

1. Introduction

The Paleocene–Eocene Thermal Maximum (PETM; ~55.8 Ma) is a rapid warming of the ocean/atmosphere system, characterized by a negative carbon isotope excursion (CIE) in both marine and terrestrial carbon (Bowen et al., 2004; Zachos et al., 2001). The onset of the PETM occurred within <10 kyr and lasted ~200 kyr (Murphy et al., 2010; Rohl et al., 2007). Foraminiferal $\delta^{18}\text{O}$ and Mg/Ca records and distributions of terrestrial and marine archaeal lipids indicate warming of up to a 3 to 8 °C in deep-sea and mid-latitude surface waters (Kennett and Stott, 1991; Weijers et al., 2007; Zachos et al., 2003, 2006), and ~5 °C warming in Arctic surface waters (Sluijs et al., 2006).

The CIE is indicative of a massive input of ^{13}C -depleted carbon that lowered ocean carbonate saturation, resulting in shoaling of the lysocline depth and dissolution of carbonates (Zachos et al., 2005; Zeebe et al., 2009). Proposed explanations for carbon input(s) include enhanced mantle CO_2 outgassing (Bralower et al., 1997; Eldholm and Thomas, 1993), dissociation of methane gas hydrates (Dickens et al., 1995, 1997; Kennett and Stott, 1991), biomass burning (Kurtz et al., 2003), intrusive-heating of organic-rich marine sediments and subsequent formation and release of methane (Svensen et al., 2004), and drying of restricted seaways leading to oxidation of organic matter (Higgins and Schrag, 2006).

The character of the CIE is a key variable in determining the carbon flux responsible for the PETM. However, a range of environmental and biologic factors can influence the $\delta^{13}\text{C}$ values of marine and terrestrial PETM records (Bowen et al., 2004; Pagani et al., 2006; Schouten et al., 2007; Smith et al., 2007). For example, PETM records from benthic foraminifera and bulk marine carbonate show a CIE magnitude of –2 to –2.5‰ (Kennett and Stott, 1991; Thomas et al., 2002), while $\delta^{13}\text{C}$ records from planktonic foraminifera often show larger CIEs, ranging –2.5 to –4‰ (Handley et al., 2008;

* Corresponding author at: University of Utah, Department of Biology, Salt Lake City, UT, 84105, United States.

E-mail addresses: brett.tipple@utah.edu (B.J. Tipple), mark.pagani@yale.edu (M. Pagani), srinath.krishnan@yale.edu (S. Krishnan), sitindra.dirghangi@yale.edu (S.S. Dirghangi), s.galeotti@uniurb.it (S. Galeotti), claudia.agnini@unipd.it (C. Agnini), luca.giusberti@unipd.it (L. Giusberti), domenico.rio@unipd.it (D. Rio).

Thomas et al., 2002; Zachos et al., 2006). Marine organic carbon and dinocyst $\delta^{13}\text{C}$ records yield larger, more negative carbon isotope excursions between -2.8‰ and -6‰ (Bolle et al., 2000; Kaiho et al., 1996; Magioncalda et al., 2004; Sluijs et al., 2007b), similar to terrestrial bulk organic carbon and carbonates that range -2.5 to -6‰ (Bowen et al., 2001; Cui et al., 2011; Koch et al., 1995; Magioncalda et al., 2004), while $\delta^{13}\text{C}$ records of terrestrial leaf-waxes range -2.8 to -6‰ (Handley et al., 2008; Pagani et al., 2006; Smith et al., 2007). Larger CIEs in terrestrial records have been explained in terms of increased photosynthetic fractionation resulting from increased humidity and soil moisture (Bowen et al., 2004) and shifts in plant types (Smith et al., 2007). However, an evaluation of plant functional-types and their carbon isotope relationships argue for an atmospheric excursion of $\sim -4.5\text{‰}$ (Diefendorf et al., 2010), in line with the CIE observed in the majority of terrestrial $\delta^{13}\text{C}$ records. Understanding subtle isotopic differences between these records is important in determining carbon cycle dynamics, as well as an accurate mass and source of the carbon responsible for the warming (McInerney and Wing, 2011).

In addition to a massive release of ^{13}C -depleted carbon at the PETM, a rapid rise in temperature occurs in near-concert with aberrations in the hydrologic cycle (Bowen et al., 2004; Pagani et al., 2006) and substantial changes in marine and terrestrial ecosystems (Collinson et al., 2009; Greenwood and Wing, 1995; Thomas et al., 1999; Wilf, 2000; Wing and Harrington, 2001; Wing et al., 2005). In general, the PETM was more humid with higher weathering rates inferred from clay mineralogy of shallow marine and terrestrial sediments (Bolle and Adatte, 2001; Clechenko et al., 2007; Cramer et al., 1999; Crouch et al., 2003; Gibson et al., 2000; Johns et al., 2008; Kopp et al., 2009; Robert and Chamley, 1991; Robert and Kennett, 1994; White and Schiebout, 2008), with evidence for extreme seasonal precipitation in some localities (Schmitz and Pujalte, 2003, 2007; Sluijs et al., 2006).

For this work, we established carbon and hydrogen isotope compositions of higher-plant derived *n*-alkanes with bulk organic carbon and marine carbonate isotope ratios from orbitally tuned, marine sediments of the Forada section in northern Italy during the PETM. Although the Forada section was shallower than the majority of studied PETM marine sections, the region did not completely escape some carbonate dissolution during the PETM—a testament to the enormous mass of carbon released. While dissolution appears to have affected marine carbonates, other geochemical and sedimentological properties suggest that the Forada record is complete and continuous, lacking the hiatus associated with carbonate burn-down (Giusberti et al., 2007). Given the limited number of expanded and continuous Paleocene–Eocene boundary sections, the Forada section is an exceptional locality for direct comparison between marine and terrestrial geochemical signatures within a single sedimentary section. Accordingly, we use our new isotope and compound-abundances records to evaluate the relative relationships between hydrologic cycle, temperature, and changes in the terrestrial and marine environments.

2. Materials and methods

2.1. Geologic setting and sampling

The Forada section, located in the Venetian pre-Alps region of northern Italy along Forada Creek (46.036083°N , 12.063975°E), is a continuous (62 m) outcropping of well-exposed pelagic to hemipelagic limestones, marls, and claystones spanning the Upper Cretaceous to the lower Eocene. PETM sediments were deposited in a near-continental environment in the western Tethys Ocean with a paleo-depth estimated between 600 and 1000 m, and no deeper than 1500 m (Giusberti et al., 2007). Tectonic deformations were less severe than elsewhere in the Alps (Channell and Medizza, 1981),

making the pre-Alps suited for studies of the lower Paleogene pelagic record (Giusberti et al., 2007).

Sixty-five samples (500–700 g) were collected spanning roughly 6 m of Paleocene–Eocene boundary section exposed in Forada Creek (Fig. 1). The section was trenched, removing ~ 50 – 75 cm of surface sediment, to unweathered rock, and samples were taken at approximately 10 cm resolution in the Eocene clay-marl unit (CMU) and marl-limestone couplets and at 5 cm resolution in the latest Paleocene marls and limestones. Samples were collected with clean instruments, wrapped in baked aluminum foil, and stored in low-bleed Whirl-pak bags prior to extraction.

2.2. Sample extraction and separation

Sediments were freeze-dried, powdered (~ 500 g), and extracted for 24 h with dichloromethane (DCM):methanol (2:1, v/v) using a Soxhlet extractor. Total lipid extracts were concentrated under a stream of purified nitrogen using a Zymark Turbovap II evaporator, transferred to 4 ml vials, and further evaporated under a gentle stream of N_2 gas. Extracts were then separated by column chromatography using 1 g deactivated silica gel (70–230 mesh) in an ashed Pasteur pipette, and eluted with 2 ml hexane, 4 ml dichloromethane and 4 ml of methanol to obtain the aliphatic, aromatic, and polar hydrocarbons, respectively. *Normal*-alkanes were further purified from cyclic and branched alkanes using urea adduction following (Wakeham and Pease, 1992).

2.3. Compound abundance and characterization

Normal-alkane abundances were determined using a Thermo Trace 2000 gas chromatograph (GC) fitted with a programmable-temperature vaporization injector and flame ionization detector (FID). Samples were processed with a fused silica, DB-1 phase column ($60\text{ m} \times 0.25\text{ mm I.D.}$, $0.25\ \mu\text{m}$ film thickness) with helium as the carrier at a flow of 2 ml/min. GC oven temperature program was 60–

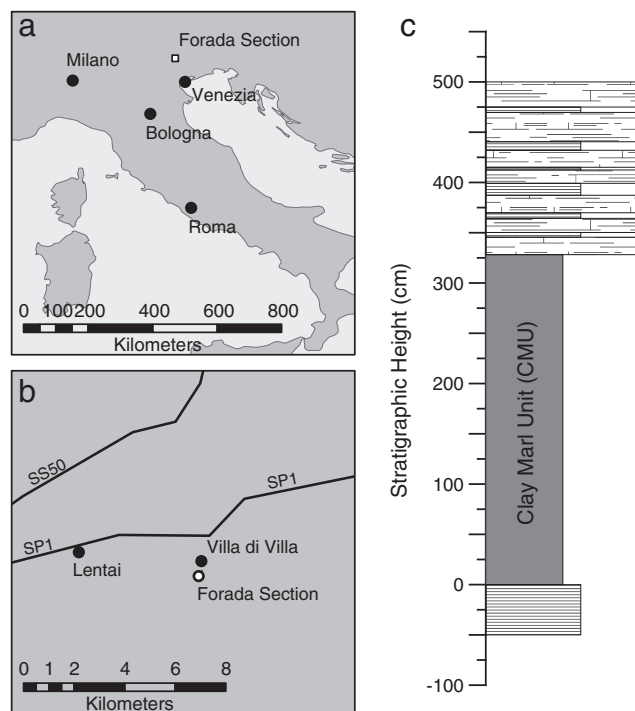


Fig. 1. Location maps and generalized stratigraphy. Regional map (a) outlining the position (white square) of the local map (b) surrounding the Forada Section and nearby towns. Generalized stratigraphy of the Forada section (c).

320 °C at 10 °C/min and isothermal for 30 min. *Normal*-alkanes were identified through comparison of elution times with known *n*-alkane standards.

Individual *n*-alkane peak areas were calculated using Xcaliber software version 1.5. Changes in average higher plant chain length (AHPCL) were calculated using the following relationship:

$$\text{AHPCL} = \frac{(A_{27}(27)) + (A_{29}(29)) + (A_{31}(31))}{(A_{27} + A_{29} + A_{31})} \quad (1)$$

where A corresponds to the area of the individual *n*-alkane peak from the chromatograph trace.

Biomarker identification and abundance were determined using a Thermo Trace 2000 gas chromatograph (GC) fitted with a split/splitless injector (splitless mode, 300 °C). Samples were processed with a fused silica, DB-5 phase column (30 m × 0.25 mm I.D., 0.25 μm film thickness) with helium as the carrier at a flow of 1.5 ml/min. GC oven temperature program was 60–320 °C at 5 °C/min and isothermal for 30 min. A Thermo Trace MS was used for detection with the mass spec scanning from 50 to 800 m/z or exclusively m/z of 191, 217, 218, 370, 372, 386, and 400 for single ion monitoring. Biomarkers were identified by elution time and mass spectra of in-house petroleum standards with published biomarker distributions (Peters et al., 2005).

2.4. Compound-specific isotope analysis

Isotope analyses were performed using a Thermo Trace 2000 GC coupled to a Finnigan MAT 253 isotope ratio mass spectrometer interfaced with a GC-C III combustion system or a High Temperature Conversion system for δ¹³C and δD analyses, respectively. The H₃⁺ factor was determined daily prior to standard calibration and sample analysis for δD measurements. GC column, carrier flow, and ramp conditions were identical to above.

Isotopic compositions were calculated following:

$$\delta = \left[\left(\frac{R_{\text{samp}}}{R_{\text{std}}} \right) - 1 \right] \times 10^3 \quad (2)$$

where R represents the ¹³C/¹²C and D/H abundance ratio, and R_{samp} and R_{std} represent the sample and standard, respectively. δ¹³C and δD values are expressed relative to Vienna Pee Dee belemnite (VPDB) and Vienna Standard Mean Ocean Water (VSMOW), respectively, based on an in-house reference gas calibrated against OzTech standard gasses.

Peaks were quantified using Isodat 2.5 and an individual baseline for both carbon and hydrogen measurements. Individual *n*-alkane isotope ratios were corrected to *n*-alkane reference materials (for δ¹³C, C₂₀, C₂₅, C₂₇, C₃₀, and C₃₈ of known isotopic ratio and for δD, “Mix A” from Arndt Schimmelmann, Indiana University) analyzed daily at several concentrations. In addition, H₂ reference gas of known isotopic composition was pulsed between sample *n*-alkane peaks to confirm if normalizations were appropriate. Standard deviations (SD) of *n*-alkane reference materials were ± 0.6‰ for δ¹³C and ± 6‰ for δD.

2.5. Bulk carbonate

Powdered samples (~300–500 mg) were weighed into a 10 ml Exetainer round-bottomed tube and sealed with butyl rubber septa. Tubes were flushed with high purity He for 700 s using a PAL auto-sampler equipped with a double-holed needle. Flushed samples were reacted with 0.2 mL of 100% orthophosphoric acid at 26 °C. One hour after the addition of the acid, CO₂ gas was sampled from the headspace and introduced to a Thermo Finnigan Delta XP isotope ratio mass spectrometer. For an individual analysis, three pulses of

house CO₂ reference gas were introduced followed by eight injections of sample gas and a final reference CO₂ pulse. δ¹³C values of six individual sample peaks (not including first and last peaks) were calculated and averaged carbonate carbon isotope value (δ¹³C_{carbonate}). Standard deviation for δ¹³C_{carbonate} determinations using international reference materials (NBS-18 and NBS-19) was ± 0.1‰.

2.6. Bulk organic carbon and nitrogen isotope ratios

250 milligrams of powdered sample was placed in a 50 ml Falcon brand centrifuge tube. 30 ml of 1N HCl was added and agitated with a vortex mixer, covered with baked aluminum foil, and placed on a 40 °C hot plate for 12 h to ensure complete dissolution of carbonates. The acidic slurry was diluted with distilled de-ionized (DDI) water, centrifuged, and decanted until a neutral solute pH was achieved. Sample residues were rinsed with approximately 100 ml of DDI water. Residues were dried by placing them in a 65 °C oven for 3 days and loosely covered with aluminum foil. Once dried, residues were weighed into tin capsules and analyzed on a Thermo Finnigan Delta^{plus} Advantage isotope ratio mass spectrometer with a Costech Elemental Analyzer and zero-blank autosampler attached. Stable isotope ratios for laboratory reference materials used during CN analysis were calibrated using NBS-19 and atmospheric N. The standard deviations of repeated measurements of reference analyses were 0.3‰ for C and 0.1‰ for N.

2.7. Glycerol dialkyl glycerol tetraether analysis

The polar glycerol dialkyl glycerol tetraether (GDGT) fraction was purified on a 2 g alumina oxide column using DCM:Methanol (1:1, v/v). The GDGT fraction was dried under a stream of purified N₂ gas, dissolved in hexane:isopropanol (99:1, v/v), and then passed through a 0.4 μm PTFE filter. Samples were analyzed and quantified by high performance liquid chromatography/atmospheric pressure chemical ionization mass spectrometer on an Agilent single quadrupole LC/MS 6100 series following instrument methods outlined in Schouten et al. (2007). PETM GDGT estimates of temperature were established using the calibration of Kim et al. (2010):

$$\text{SST} = 81.5 \times \text{TEX}_{86} - 26.6, \quad (3)$$

where

$$\text{TEX}_{86} = \frac{[\text{GDGT}-2] + [\text{GDGT}-3] + [\text{Cren}']}{[\text{GDGT}-1] + [\text{GDGT}-2] + [\text{GDGT}-3] + [\text{Cren}']} \quad (4)$$

where Cren' indicate the crenarchaeol regio-isomer and GDGT-1, GDGT-2 and GDGT-3 indicate GDGTs containing 1, 2, and 3 cyclopentane moieties, respectively (Kim et al., 2010). Other GDGT-SST calibrations are provided in the Supplemental materials. A round-robin analysis of GDGT compounds between Yale University, Royal Netherlands Institute for Sea Research, and Harvard University produced temperature estimates within 1 °C of one another for the TEX₈₆ index. Internal reproducibility of calculated temperature is within 1.5 °C for all analysis.

3. Results

3.1. Sediment thermal maturity

A subset (n=11) of the thirty-three Forada extracts from throughout the stratigraphic section was analyzed to assess thermal maturity as thermal alteration of organic matter can alter the isotopic composition through exchange of carbon-bound hydrogen. Here we evaluate the thermal maturity of Forada sediments using established hopane and sterane isomerization indices (Peters et al., 2005). Given

the relatively condensed stratigraphic sequence (~6 m), it was not necessary to analyze all samples as all samples were likely exposed to similar thermal stresses, and indeed, we observed little variation in thermal maturity throughout the section. Stereoisomers of Tm and Ts C₂₇ hopanes were identified. Forada Ts/Ts + Tm values averaged 0.13 and range between 0.03 and 0.23. In all samples the less stable C₂₇ hopane (Tm) in much greater concentrations than the more stable Ts, suggesting low thermal maturity. Ts/Ts + Tm values below 0.35 correspond to vitrinite reflectance values of 0.5 and below (Peters et al., 2005) and correspond to immature organic material. In addition, C₃₁ and C₃₂ homohopanes were in significant concentrations to measure the homohopane isomerization index 22S/22S + 22R. C₃₁–C₃₅ homohopanes have a stereocenter in the side chain at C-22 that isomerizes from the biological 20R configuration to an equilibrium mixture of the 20R and 20S diastereomers during thermal maturation. 22S/22S + 22R values averaged 0.49 and range between 0.40 and 0.55. The majority of samples had greater concentrations of the biological homohopane precursor (22R) than the geological derivative (22S). 22S/22S + 22R reaches equilibrium at ~0.60 and near the very earliest stages of oil generation temperatures. Similar to the Ts/Tm ratios, 22S/22S + 22R ratios suggest immature organic material below oil generation temperatures. Steranes were in very low abundance in Forada extracts. We found the sterane isomerization 20S/20S + 20R index for C₂₇ steranes was 0.25. 20S/20S + 20R values below 0.25 correlate to vitrinite reflectance values of ~0.5 and immature organic material.

3.2. Forada bulk carbonate and total organic carbon $\delta^{13}\text{C}$ records

Bulk carbonate content ranged between 36 and 92 weight percent (wt.%) in the latest Paleocene interval, 17–87 wt.% from 0 to 320 cm within the main body of the carbon isotope excursion and clay-marl unit (CMU), and 52–100 wt.% from 330 to 500 cm during the recovery and equilibration interval (Table S1). The interpretation that the CMU (0–320 cm) is the lithologic expression of the PETM and not a burn-

down interval, is supported by micropaleontological data, including calcareous planktonic and benthic foraminiferal biostratigraphy, (Giusberti et al., 2007). Further, sedimentation rates increase five-fold during the clay marl interval compared to the Late Paleocene, indicative of increased continental weathering and increased terrigenous input (Giusberti et al., 2007).

Latest Paleocene bulk $\delta^{13}\text{C}_{\text{carbonate}}$ values range between -0.2 and 1.2‰ with an average of 0.5‰ (Table S1). A subtle +0.8‰ shift from 0.4‰ to 1.2‰ in $\delta^{13}\text{C}_{\text{carbonate}}$ values is observed between -100 cm and -60 cm followed by a steady 1.4‰ depletion in ^{13}C from -60 cm to -2 cm (Fig. 2). The onset of the CIE is marked by an abrupt negative 2.0‰ change from -2 cm to 10 cm followed by a +1.3‰ increase between 10 cm and 30 cm. The initial spike in $\delta^{13}\text{C}_{\text{carbonate}}$ values is followed by a plateau rather than a broad shift to more negative $\delta^{13}\text{C}_{\text{carbonate}}$ values, and lithologic change from a ~0.2 cm black clay interval followed by a 320 cm thick gray-green (0.2–50 cm) and reddish (50–320 cm) clay marl interval is associated with the base of the Eocene. $\delta^{13}\text{C}_{\text{carbonate}}$ values remain near -1.0‰ from 30 cm until 260 cm where $\delta^{13}\text{C}$ values become 0.9‰ more negative for 50 cm (270–320 cm). A distinct lithologic change from gray-green marls to limestone-red marl couples occurs at 330 cm with a corresponding shift in $\delta^{13}\text{C}_{\text{carbonate}}$ values from -1.3 to -0.2‰. $\delta^{13}\text{C}_{\text{carbonate}}$ values steadily become more positive reaching 0.7‰ for the remainder of the section.

$\delta^{13}\text{C}_{\text{organic}}$ values range between -24.8 and -30.2‰ with an average value of -26.4‰ (Table S1). Latest Paleocene $\delta^{13}\text{C}_{\text{organic}}$ values average -25.1‰ (Fig. 2). The onset of the CIE represented by the $\delta^{13}\text{C}_{\text{organic}}$ record is marked by an abrupt -3.1‰ change from -15 cm to 5 cm followed by a +1.7‰ shift between 5 cm and 10 cm. As with the $\delta^{13}\text{C}_{\text{carbonate}}$ record, the onset of the CIE is marked by a spike in $\delta^{13}\text{C}_{\text{organic}}$ values followed by a plateau rather than a general shift to more negative $\delta^{13}\text{C}_{\text{organic}}$ values. $\delta^{13}\text{C}_{\text{organic}}$ values remain ~-26.0‰ from 10 to 200 cm where values become 0.9‰ more negative for 60 cm (260–310 cm). $\delta^{13}\text{C}_{\text{organic}}$ values trend more positive by 1.0‰ for the remainder of the

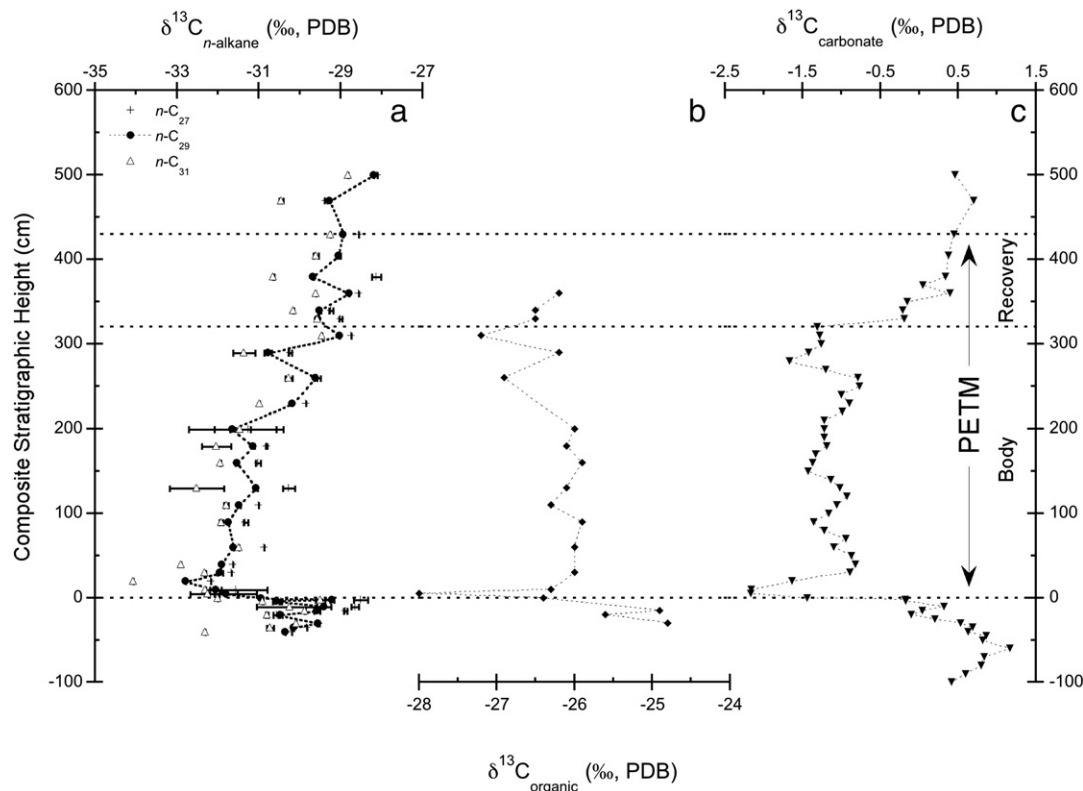


Fig. 2. Stable carbon isotope ratios of higher plant *n*-alkanes (a), bulk organic carbon (b) and bulk carbonates (c) for the Paleocene–Eocene boundary interval in Forada. Terrestrial higher plant *n*-C₂₇, *n*-C₂₉, and *n*-C₃₁ $\delta^{13}\text{C}$ values are shown as crosses, closed circles, and triangles, respectively.

section coupled with a lithologic change from marls to limestone-red marl couplets at 320 cm.

3.3. Forada terrestrial higher-plants records: $\delta^{13}\text{C}$, δD , and compound-distributions

Saturated hydrocarbons are dominated by a homologous series of *n*-alkanes from *n*-C₂₃ to *n*-C₃₅, with *n*-C₂₇, *n*-C₂₉, and *n*-C₃₁ as the most abundant compounds. Normal-alkanes are characterized by an odd-over-even character consistent with terrestrial higher-plant derived materials (Eglinton and Hamilton, 1967) with a CPI value of greater than 2 for all samples. We restrict our analysis and discussion to records expressed by *n*-C₂₇, *n*-C₂₉, and *n*-C₃₁.

Stable carbon isotope values of individual *n*-alkanes ($\delta^{13}\text{C}_{n\text{-alkane}}$) range from -28.1% to -34.1% with an average value -30.5% (Table 1). In individual samples, $\delta^{13}\text{C}_{n\text{-alkane}}$ values are generally more ^{13}C -depleted as chain-length increases, similar to relationships that characterize modern plant leaf waxes (Bi et al., 2005; Collister et al., 1994; Zhou et al., 2010). The $\delta^{13}\text{C}_{n\text{-alkane}}$ of all *n*-alkanes trend toward more negative above -2 cm in the Forada section (Fig. 2) corresponding to the CIE expressed by the $\delta^{13}\text{C}_{\text{carbonate}}$ record. Latest Paleocene $\delta^{13}\text{C}_{n\text{-alkane}}$ values of *n*-C₂₇, *n*-C₂₉, and *n*-C₃₁ range from -28.5 to -30.6% , -29.2 to -30.6% , and -29.5 to -32.3% , respectively. From 0 cm to 20 cm, *n*-C₂₇, *n*-C₂₉, and *n*-C₃₁ $\delta^{13}\text{C}_{n\text{-alkane}}$ values become more negative (-32.2% , -32.8% , and -34.1%), thus the magnitude of the CIE for the Forada $\delta^{13}\text{C}_{n\text{-alkane}}$ record is 3.7‰, 3.6‰, and 4.6‰, respectively. Following the onset of the CIE, *n*-C₂₇, *n*-C₂₉, and *n*-C₃₁ $\delta^{13}\text{C}_{n\text{-alkane}}$ values show a steady progression toward pre-event values within the main body of the CIE and average -30.9% , -31.3% , and -31.8% , respectively. The $\delta^{13}\text{C}_{n\text{-alkane}}$ values during the recovery

phase (as characterized by lithologic changes and $\delta^{13}\text{C}_{\text{carbonate}}$ variations) and post-event intervals are similar to pre-excursion $\delta^{13}\text{C}$ values.

Stable hydrogen isotope values of *n*-alkanes ($\delta\text{D}_{n\text{-alkane}}$) range from -126% to -153% over the studied interval (Table 1). Low molecular concentrations limit the number of possible $\delta\text{D}_{n\text{-alkane}}$ measurements compared to $\delta^{13}\text{C}_{n\text{-alkane}}$ values. However, the entire PETM and pre-event intervals were sampled at higher resolution compared to other *n*-alkane hydrogen records (Fig. 3). Prior to the onset of the CIE at 0 cm, $\delta\text{D}_{n\text{-alkane}}$ values for *n*-C₂₇ and *n*-C₂₉ become more D-enriched from -147% to -136% and -152% to -136% between -35 cm and -2 cm, respectively, while *n*-C₃₁ remains relatively constant ranging from -138% to -132% . At the onset of the CIE, $\delta\text{D}_{n\text{-alkane}}$ values for *n*-C₂₇, *n*-C₂₉, and *n*-C₃₁ immediately become more D-depleted by 6 to 9‰. Between 10 cm and 290 cm, $\delta\text{D}_{n\text{-alkane}}$ values for *n*-C₂₇, *n*-C₂₉, and *n*-C₃₁ remain relatively constant. D/H compositions of *n*-alkanes are more D-enriched above 320 cm and coincident with the recovery phase of the PETM, and stabilize to pre-event values near the end of the CIE.

Higher-plant average chain-length (AHPCL) decreases from 31.2 to 29.7 between -40 cm and -4 cm towards the onset of the CIE (Table S1, Fig. 3). From -4 cm to the beginning of the CIE, AHPCL increases to 30.8 and abruptly decreases to 29.5 at 5 cm, and then remains relatively stable between 10 and 60 cm with an average value of 29.9 and a range between 29.8 and 30.1. A shift in AHPCL occurs from 29.9 to 31.0 between 60 cm and 90 cm with values near 31 from 90 to 300 cm. After 300 cm to the end of the CIE, AHPCL gradually decreases from 31.0 to 30.0 corresponding to the recovery phase.

A subset ($n=11$) of the thirty-three Forada extracts from throughout the stratigraphic section was subjected to detailed higher-plant biomarker analysis. Here we assess higher-plant input to

Table 1
Forada *n*-alkane carbon and hydrogen isotope values with stratigraphic height and age.

Stratigraphic height (cm)	kyr before/after PETM onset	Carbon isotope values (‰, PDB)						Hydrogen Isotope values (‰, VSMOW)		
		<i>n</i> -C ₂₇	<i>n</i> -C ₂₇ SD	<i>n</i> -C ₂₉	<i>n</i> -C ₂₉ SD	<i>n</i> -C ₃₁	<i>n</i> -C ₃₁ SD	<i>n</i> -C ₂₇	<i>n</i> -C ₂₉	<i>n</i> -C ₃₁
500	246.7	-28.1		-28.2		-28.8				
470	222.2	-29.4	0.0	-29.3	0.0	-30.5	0.0			
430	196.2	-28.6		-29.0		-29.3				
405	175.5	-29.1	0.0	-29.1	0.1	-29.6	0.1	-142	-134	-126
380	154.3	-28.1	0.1	-29.7	0.0	-30.7	0.0			
360	134.1	-28.6		-28.8		-29.6				
340	116.5	-29.2	0.0	-29.5	0.0	-30.2	0.0	-135	-133	-130
330	108.8	-29.0	0.0	-29.6	0.0	-29.6	0.0	-136	-138	-130
310	98.7	-28.8		-29.0		-29.5				
290	90.3	-30.2	0.0	-30.8	0.1	-31.4	0.3	-146	-146	-145
260	79.0	-29.6	0.1	-29.6	0.0	-30.3	0.1	-141	-140	-135
230	68.9	-29.9			-30.2	-31.0				
200	59.5	-31.3	0.8	-31.7	1.1	-31.5	0.3			
180	53.9	-30.8	0.0	-31.2	0.0	-32.0	0.4	-144	-150	-149
160	48.3	-31.0	0.1	-31.5	0.0	-32.0	0.0	-143	-146	-147
130	40.0	-30.3	0.1	-31.1	0.0	-32.5	0.7	-147	-150	-153
110	34.8	-31.0	0.0	-31.5	0.0	-31.8	0.1	-138	-147	-148
90	29.5	-31.3	0.1	-31.8	0.0	-31.9	0.0	-139	-145	-146
60	21.7	-30.9		-31.6		-31.5				
40	14.6	-31.6		-31.9		-32.9				
30	11.0	-31.7	0.0	-32.0	0.1	-32.3	0.0			
20	7.3	-32.2		-32.8		-34.1				
10	3.7	-31.6	0.8	-32.1	0.1	-32.3	0.0	-142	-144	-141
5	1.8	-31.5	0.5	-31.8	0.3	-32.3	0.4			
0	0.0			-30.9		-32.0				
-2	-1.9	-28.5	0.2	-29.2	0.1	-29.5	0.1	-136	-136	-135
-4	-3.8	-30.5	0.0	-30.6	0.1	-30.9	0.0	-128	-133	-134
-10	-9.5	-28.7	0.1	-29.4	0.2	-30.3	0.8			
-15	-14.3	-28.9	0.0	-29.6	0.1	-29.9	0.0	-146	-140	-133
-20	-19.1	-30.6	0.1	-30.5	0.0	-30.8	0.0	-153	-142	-134
-30	-28.6	-29.5	0.0	-29.6	0.0	-30.1	0.0	-138	-140	-137
-35	-33.4	-29.8	0.0	-30.2		-30.7	0.1	-147	-152	-138
-40	-38.2	-30.2		-30.4		-32.3				

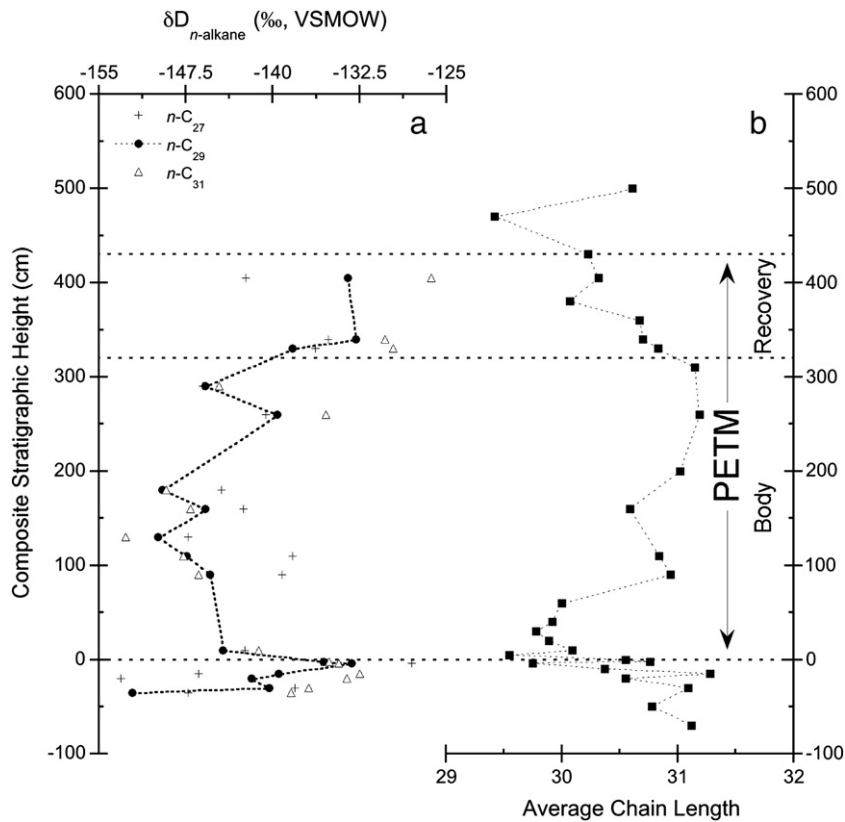


Fig. 3. Stable hydrogen isotope ratios of higher plant n -alkanes (a) with higher plant average chain length values (b) for Forada sediments. Terrestrial higher plant n -C₂₇, n -C₂₉, and n -C₃₁ δ D values are shown as crosses, closed circles, and triangles, respectively.

the Forada sediments and variations in angiosperm- and gymnosperm-specific molecules. Cadalene, derived from higher-plants, were observed in all samples with no significant abundance variation. While only observed in several samples, higher-plant specific dihydro-ar-cucumene was also present. Angiosperm-specific bicadinenes, 1,2,5, and 1,2,7-trimethylnaphthalenes, olenane, and tetra-aromatic der beta amyryn were also targeted. Bicadinenes were observed in 6 of the 11 samples with no significant abundance variation throughout the section while no other angiosperm-specific biomarkers were detected. Gymnosperm-specific Simonellite, Retene, and dehydroabietane were also targeted with none detected in any Forada fraction analyzed.

3.4. Paleocene–Eocene sea-surface temperature estimates

Recovery of the GDGT fraction was low for all samples extracted. Of the 35 samples extracted and analyzed, 15 samples yielded measurable GDGT concentrations (Table S1). The BIT index ranged from 0.660 to 0.997, suggesting significant contribution of terrestrial soil organic material (Hopmans et al., 2004) and consistent with interpretations of increased continental weathering and terrigenous input to the Forada section (Giusberti et al., 2007). The highest BIT index values occur near the onset of the CIE (−4 cm to 10 cm) suggesting the largest influx of terrestrial soil organic matter to the Forada sediment occurred at the start of the PETM. Given the elevated BIT values temperature estimates should be regarded as qualitative, however estimates of Latest Paleocene temperatures gradually increase from 29 to 32 °C toward the onset of the CIE. A slight decrease in temperature estimates occur at the onset of the CIE, followed immediately by a 4 °C increase. During the body of the event temperatures remain between 27 and 32 °C. While the absolute temperatures are qualitative, given the elevated BIT values throughout the section the temperature trends are likely valid.

4. Discussion

4.1. A comparison of Forada PETM carbonate, bulk organic, and terrestrial carbon $\delta^{13}\text{C}$ records

The Forada marine $\delta^{13}\text{C}_{\text{carbonate}}$ record is broadly similar to other marine carbonate $\delta^{13}\text{C}$ records (Bains et al., 1999) except for the presence of a sharp positive shift in $\delta^{13}\text{C}_{\text{carbonate}}$ immediately following the onset of the CIE (Bains et al., 1999; Cramer et al., 2003; Zachos et al., 2005). A $\delta^{13}\text{C}$ spike at the initial onset of the CIE is observed in surface-dwelling foraminifera (Kennett and Stott, 1991; Thomas et al., 2002) and terrestrial records (Bains et al., 2003; Bowen et al., 2001), but not in bulk marine carbonates. The absence of a carbon isotope shift in bulk carbonate records is explained by the extent of dissolution, or changes in carbonate fraction, or as a true reflection of regional paleoceanographic characteristics (Stoll, 2005). Bulk carbonate $\delta^{13}\text{C}$ value at Forada become 1.3‰ more positive following the initial 2‰ negative carbon isotope excursion, similar to +1–2‰ changes observed in both Polecat Bench carbonate nodules (Bains et al., 2003) and Site 690 planktonic foraminifera (Bains et al., 2003; Kennett and Stott, 1991; Thomas et al., 2002). The Forada $\delta^{13}\text{C}_{\text{organic}}$ and $\delta^{13}\text{C}_{n\text{-alkane}}$ records are similar to the coeval $\delta^{13}\text{C}_{\text{carbonate}}$ record, displaying an abrupt shift following the initiation of the CIE (Fig. 2). These observations are consistent with trends from other high-resolution PETM records and carbon cycle models that predict a sharp negative spike followed by a subtle enrichment in surface- and deep-ocean carbon pools associated with the initial input of ^{13}C -depleted CO_2 (Zeebe et al., 2009).

The Forada $\delta^{13}\text{C}_{\text{carbonate}}$ record is similar to other marine bulk CIE records including the presence of a discrete onset, body or plateau, and recovery phase. In contrast, the Forada $\delta^{13}\text{C}_{n\text{-alkane}}$ record shows a clear onset of the CIE, a subtle and gradual ^{13}C -enrichment during the main body, and a sharp return to pre-event $\delta^{13}\text{C}$ values immediately

following initiation of the recovery phase. Isotopic differences between these records can be explained in a variety of ways. Leaf waxes are produced throughout the growing season (Pedentchouk et al., 2008; Sachse et al., 2009) and transported to isolated marine settings on the order of days, weeks to years (Conte and Weber, 2002). Carbon-14 dating of fluvial and aeolian transported organic carbon and *n*-alkanes show these carbon pools are a mix of ancient and modern components (Drenzek et al., 2007; Eglinton et al., 1997; Raymond and Bauer, 2001). Comparison of compound-specific and bulk ^{14}C ages from varved marine sediments show that total organic carbon and *n*-alkanes are 500–4000 yr older than the calendar age of the sediments (Smittenberg et al., 2004). Thus, ^{14}C ages of organic compounds represent a mixture of modern sources and more ancient organic carbon that reflects the mean reservoir storage time in soils prior to erosion and deposition in the basin (Smittenberg et al., 2004). As a result, the $\delta^{13}\text{C}_{n\text{-alkane}}$ CIE should manifest differently between localities. Accordingly, we interpret the Forada $\delta^{13}\text{C}_{n\text{-alkane}}$ record as a mixture of ^{13}C -depleted PETM *n*-alkanes and older ^{13}C -enriched Paleocene soil/sedimentary *n*-alkanes.

High-resolution chronologies have been developed for ODP Site 690 and Leg 208 (Murphy et al., 2010; Rohl et al., 2000, 2007) along with the onshore marine Forada section (Giusberti et al., 2007). Rohl et al. (2007) and Giusberti et al. (2007) disagree on the duration of the main excursion and recovery interval in Forada (179 ± 17 kyr and 231 ± 22 kyr, respectively). The main difference between these two chronologies is the assignment of different numbers of precessional cycles within the main body and recovery interval. However, a recent ^3He -based chronology from Leg 208 suggest a total PETM duration of $234^{+48}/_{-34}$ kyr (Murphy et al., 2010) in line with the cycle-based Forada age model of Giusberti et al. (2007), these models are inline with recent age models of Bowen and Zachos (2010). For this study, we use the age model of Giusberti et al. (2007) for Forada and assume a constant sedimentation rate within the individual precessional cycles. Here the first precessional cycle observed in Forada is from 0 to 57 cm and we find a lag between the initial peaks in $\delta^{13}\text{C}_{\text{carbonate}}$ and $\delta^{13}\text{C}_{n\text{-alkane}}$ of 10–15 cm. Given this, the $\delta^{13}\text{C}_{n\text{-alkane}}$ record at Forada appears delayed $\sim 4\text{--}5$ kyr relative to the $\delta^{13}\text{C}_{\text{carbonate}}$ record within the considered precessional cycle. These data suggest the average residence time of *n*-alkanes delivered to Forada sediments to be at least 4000 yr (Fig. 4). In addition, we find the $\delta^{13}\text{C}_{\text{carbonate}}$ and $\delta^{13}\text{C}_{\text{organic}}$ responses equivalent, suggesting the bulk marine carbonate and organic carbon pools are coupled (Fig. 4), a supposition supported by bulk organic matter C/N ratios ranging between 2 and 4 (Meyers, 1994). While bioturbation and sediment mixing may have altered the Forada records, the similarity between the $\delta^{13}\text{C}_{\text{carbonate}}$ and $\delta^{13}\text{C}_{\text{organic}}$ responses suggest mixing affected each record equally and indicate the terrestrial lag is likely genuine.

Studies of modern soils suggest *n*-alkanes are highly recalcitrant within developed soils with *n*-alkane ages and soil depth linearly related (Huang et al., 1999). Radiocarbon ages suggest *n*-alkanes in soils can be up to 15,000 yr older than the modern (Bol et al., 1996; Huang et al., 1999; Paul et al., 1997). Thus, under higher weathering rates associated with the PETM, weathering and deposition of older *n*-alkanes is anticipated. Deeper weathering of old Paleocene-aged *n*-alkanes likely contributed to the increase in the age of the average *n*-alkane deposited in Forada sediments.

At any locality, the relative proportion of contemporaneous *n*-alkanes and older ^{13}C -enriched Paleogene soil/sedimentary *n*-alkanes could vary as hydrology and weathering evolve during the climate event. For example, the entire Forada CMU interval has been interpreted to reflect a period of increased terrigenous flux that monotonically decreased after the onset of the CIE (Giusberti et al., 2007). If hydrologic changes and its influence on the transport of pre-PETM *n*-alkanes impacted the $\delta^{13}\text{C}_{n\text{-alkane}}$ record, then a gradual CIE onset followed by a plateau in Forada $\delta^{13}\text{C}_{n\text{-alkane}}$ values is expected. However, this is not observed (Fig. 2) and suggests

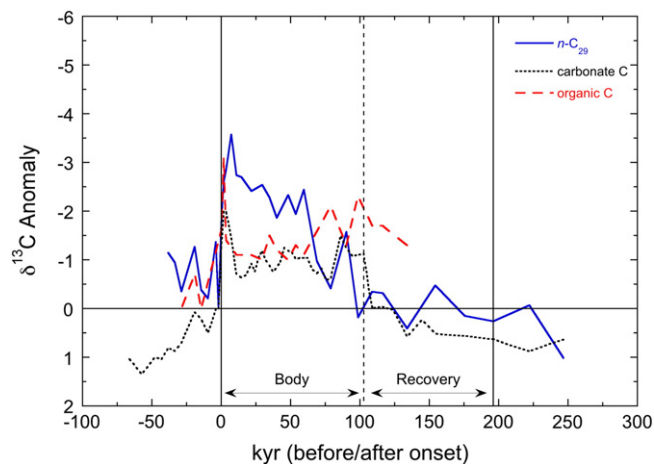


Fig. 4. Normalized carbon isotope excursions from the Forada *n*-alkane, carbonate, and organic carbon records. Trends for *n*-C₂₉, carbonates, and organic carbon $\delta^{13}\text{C}$ values are shown with blue, dotted, and red lines, respectively. The PETM is outlined with solid lines with the main body and recovery intervals delineated by a dashed line. (For interpretation of the references to color in this figure legend, the reader is referred to the web version of this article.)

variations in the relative residence time of *n*-alkanes did not substantially change during the PETM.

Large changes in plant communities have been invoked to explain differences between terrestrial *n*-alkane and marine $\delta^{13}\text{C}$ PETM records (Schouten et al., 2007; Smith et al., 2007). The majority of terrestrial higher plants produce *n*-alkanes, and while some species produce unique *n*-alkane finger-prints (Eglinton and Hamilton, 1967), many unrelated species within a single ecosystem can have similar or overlapping *n*-alkane distributions. Further, *n*-alkanes and biomarker $\delta^{13}\text{C}$ values of angiosperms are $\sim 1\text{--}2\%$ more negative than gymnosperms (Schouten et al., 2007) suggesting that variations in $\delta^{13}\text{C}_{n\text{-alkane}}$ values could be related to changes in the relative inputs of gymnosperm and angiosperm sources. To resolve these issues, *n*-alkane isotope records have been combined with pollen abundance (Stuijs et al., 2007b), source-specific biomarkers (Schouten et al., 2007) and microfossil studies (Smith et al., 2007) to interpret ancient terrestrial records. However, *n*-alkanes (aeolian, fluvial), terpenoid biomarkers (fluvial), microfossils (fluvial) and pollen (aeolian, fluvial) have different taphonomic transport pathways to marine and terrestrial sediments (Schouten et al., 2007), and these differences can introduce biases through incorporation of reworked pollen and biomolecules. Furthermore, these terrestrial records can have different temporal responses to climate events, similar to the temporal difference observed between the Forada marine and terrestrial $\delta^{13}\text{C}$ records. However, changes in terrestrial plant communities undoubtedly accompanied climate change in the Forada section's input area. Subtle changes in plant communities can be interpreted from variations in the higher-plant *n*-alkane average chain length. Variations in AHPCL can occur due to plant community variations or environmental change. Environmental controls on AHPCL are not well constrained, however, increased average carbon-chain length has been related to increases in temperature and/or aridity (Sachse et al., 2006). At Forada, we observe rapid fluctuations prior to the CIE and a decrease in AHPCL immediately following the onset CIE, suggesting a decrease in aridity and/or temperature, or a large change in plant community. Given concurrent increases in global temperatures, the Forada AHPCL record likely reflects an increase in humidity and/or plant community change. Similar to the Forada $\delta^{13}\text{C}_{n\text{-alkane}}$ record, the AHPCL record should incorporate a similar lag relative to the marine records.

While we do not have concrete evidence for or against a shift in vegetation near the Forada section, it is unlikely that gymnosperms

constituted a major component of this sub-tropical ecosystem prior to, and during the PETM given that Tethyan vegetation was dominated by rainforest and evergreen angiosperms (Utescher and Mosbrugger, 2007) during the latest Paleocene to Eocene. Biomarker abundances support this argument and suggest very limited gymnosperm contributions to Forada sediments. The magnitude of the Forada $\delta^{13}\text{C}_{n\text{-alkane}}$ CIE is only -3.6 to -4.6% —smaller than other terrestrial $\delta^{13}\text{C}_{n\text{-alkane}}$ records that experience floral shifts, and thus consistent with our interpretations that a gymnosperm-to-angiosperm shift did not occur. Thus, it is possible that the Forada $\delta^{13}\text{C}_{n\text{-alkane}}$ record represents an accurate expression (while lagged) of the global CIE. An intriguing feature of the Forada $\delta^{13}\text{C}_{n\text{-alkane}}$ CIE is its resemblance to the terrestrial carbonate $\delta^{13}\text{C}$ Polecat Bench section of the Bighorn Basin, Wyoming (Bains et al., 2003; Bowen et al., 2001). For both records, most negative values occur at the base with a sharp peak, followed by a gradual return toward more ^{13}C -enriched values across the main body. The transition to the CIE recovery phase is sharp in both terrestrial records, and magnitudes of the CIE are very similar between the Forada $\delta^{13}\text{C}_{n\text{-alkane}}$, -3.5 to -4.5% and Polecat Bench $\delta^{13}\text{C}_{\text{carbonate}}$ records $\sim -4.0\%$.

4.2. CIE response: Forada compared to other n -alkane $\delta^{13}\text{C}$ records

As more compound-specific terrestrial plant $\delta^{13}\text{C}$ records are established, more questions have arisen regarding the terrestrial response to the PETM. To date, seven PETM $\delta^{13}\text{C}_{n\text{-alkane}}$ records (including this study) have been compiled spanning the tropical (Tanzania) to polar latitudes (Lomonosov Ridge) (Handley et al., 2008; Hasegawa et al., 2006; Kaiho et al., 1996; Pagani et al., 2006; Smith et al., 2007) (Crouch and Visscher, 2003; Jaramillo et al., 2010; McCarren et al., 2008). Of these six records, five are terrestrial n -alkane records extracted from marine sediments either from outcrop (Kaiho et al., 1996, this study) or sediment core samples (Handley et al., 2008; Hasegawa et al., 2006; Pagani et al., 2006), while one was developed from terrestrial paleosols outcroppings (Smith et al., 2007). Global patterns in terrestrial plant's response to the PETM are becoming apparent. Terrestrial n -alkane $\delta^{13}\text{C}$ records are depleted in ^{13}C relative to more conventional marine $\delta^{13}\text{C}$ excursions of 2 to 3‰ (CIEs based on $\delta^{13}\text{C}_{n\text{-alkane}}$ records from New Zealand, Walvis Ridge, Lomonosov Ridge, Bighorn Basin-Wyoming, Tanzania, and this study are -2.8% , -4.3 to -5.1% , 4.5 – 6% , 3.7 – 5.1% , 5.3 – 7% , and -3.6 to -4.6% , respectively). A larger CIE in terrestrial plant material has been interpreted as a response to enhanced soil moisture and humidity during the PETM (Bowen et al., 2004). Increased moisture availability reduced plant water-stress, allowing for greater ^{13}C discrimination during terrestrial photosynthesis. However, this explanation requires increases in soil moisture and temperature to overcome the competing driver on photosynthetic fractionation of increased temperature during the PETM (Bowen et al., 2004). Another model argues for changes in forest composition as a way to account for the discrepancy between marine and terrestrial $\delta^{13}\text{C}$ records (Schouten et al., 2007; Smith et al., 2007). Given that angiosperms have $\delta^{13}\text{C}_{n\text{-alkane}}$ values more negative by 1–2‰ than gymnosperms (Chikaraishi and Naraoka, 2003), an increase in angiosperms relative to gymnosperms during the PETM could account the CIE inconsistency between $\delta^{13}\text{C}$ records. While these models may be viable in particular locations and environments, they do not explain the global discrepancy observed between the terrestrial and marine carbon reservoirs as they would require global increases in photosynthetic fractionation or angiosperms. As more terrestrial CIE records become available, increased focus should be placed on explaining this discrepancy.

At Forada, we find a decoupling of the marine and terrestrial response to the CIE during the initial interval (Fig. 4). Specifically, we find the terrestrial $\delta^{13}\text{C}_{n\text{-alkane}}$ response in the initial 15 kyr lacks the $+1.3\%$ shift observed in $\delta^{13}\text{C}_{\text{carbonate}}$ record. Between 15 and 65 kyr after the CIE onset, both $\delta^{13}\text{C}_{n\text{-alkane}}$ and $\delta^{13}\text{C}_{\text{carbonate}}$ records vary in concert with the $\delta^{13}\text{C}_{n\text{-alkane}}$ record demonstrating higher variance. Finally, between 65 and 75 kyr the marine $\delta^{13}\text{C}_{\text{carbonate}}$ response lacks the $+2\%$ shift

observed in the $\delta^{13}\text{C}_{n\text{-alkane}}$ record. Thus, our new Forada record provides evidence for decoupling between marine and terrestrial responses during the initial ~ 75 kyr of the CIE. However, during the latter (>75 kyr) portion of the event, similar isotopic anomalies emerge (Fig. 4) suggesting that either the marine record was dampened and/or the terrestrial record amplified during the onset of the PETM. Further, the Forada terrestrial CIE is remarkably similar simulations that apply a single pulse of carbon to account for carbon isotope trends (Zeebe et al., 2009).

4.3. Pre-CIE hydrology change and associated plant community and temperature

We found all biomarker thermal maturity parameters to suggest immature organic material. While these biomarkers do not correspond to specific temperatures, these data suggest the sediments have not been exposed to temperatures greater than 60°C . Under these conditions we feel confident that little to no isotopic exchange of the alkyl hydrogen atoms has occurred and suggest the original biologic D/H ratios are preserved in Forada sediments.

Hydrogen isotopes of plant materials reflect a combination of isotopic effects related to photosynthetic pathways, growth forms, water-use efficiency, and the hydrogen isotope composition of source-water used during photosynthesis (Hou et al., 2007; Pedentchouk et al., 2008; Roden et al., 2000). Modern studies have shown $\delta\text{D}_{n\text{-alkane}}$ values are directly related to meteoric-water δD values, as well as rates of transpiration and soil evaporation (Chikaraishi and Naraoka, 2003; Pedentchouk et al., 2008; Sachse et al., 2006, 2009; Smith and Freeman, 2006). In general, PETM $\delta\text{D}_{n\text{-alkane}}$ records show relatively large isotopic variations (Handley et al., 2008; Pagani et al., 2006; Smith et al., 2007). $\delta\text{D}_{n\text{-alkane}}$ values from Tanzania shift to 20–40‰ more positive values at the onset of the PETM and remain relatively stable until an erosional surface limits interpretation during later portions of the PETM (Handley et al., 2008). One mid-latitude $\delta\text{D}_{n\text{-alkane}}$ record from North American continental interior, shows a 10‰ D-enrichment prior to the CIE followed by a negative shift (Smith et al., 2007), similar to trends observed in the Arctic where a large enrichment ($\sim 55\%$) was observed near the onset of the CIE followed by a return to pre-event $\delta\text{D}_{n\text{-alkane}}$ values (Pagani et al., 2006).

While plant community variation across the PETM could affect δD values, many of these δD shifts have been interpreted in terms of hydrological conditions (Handley et al., 2008; Pagani et al., 2006; Smith et al., 2007). Paleogene general circulation models indicate latitudinal variability in precipitation, with a decrease in total precipitation in low- and mid-latitudes. In higher-latitude continental regions and monsoonal climates, simulated increases in precipitation are observed (Huber and Sloan, 1999; Shellito et al., 2003). Low meridional temperature gradients lead to decreased zonal wind strength and increased tropical evaporation (Huber and Sloan, 1999). These conditions predict a decrease in the meridional isotopic gradient and D-enriched precipitation globally (Pierrehumbert, 2002), as well as smaller D/H changes in the low- to mid latitudes relative to the high latitudes (Pagani et al., 2006).

In general, $\delta\text{D}_{n\text{-alkane}}$ records are limited by resolution and erosional surfaces. Nevertheless, a broad pattern is emerging with mid- and high latitudes expressing larger negative D/H excursion near the onset of the CIE (Pagani et al., 2006; Smith et al., 2007). The Arctic record follows similar variations when updated age calibrations are used (Sluijs et al., 2007a). This trend is also expressed in the Forada $\delta\text{D}_{n\text{-alkane}}$ record where D-enrichment occurs prior to the event, followed by an abrupt and stable shift to more negative values, ending a gradual change to more positive values during the recovery phase of the PETM (Fig. 3). The shift to more positive $\delta\text{D}_{n\text{-alkane}}$ values prior to the onset of the CIE suggests early adjustments in hydrologic conditions just before the onset of the isotope anomaly. Given the limited resolution of the Forada $\delta\text{D}_{n\text{-alkane}}$ record compared the $\delta^{13}\text{C}_{n\text{-alkane}}$ record, we cannot assess temporal offsets in the hydrogen

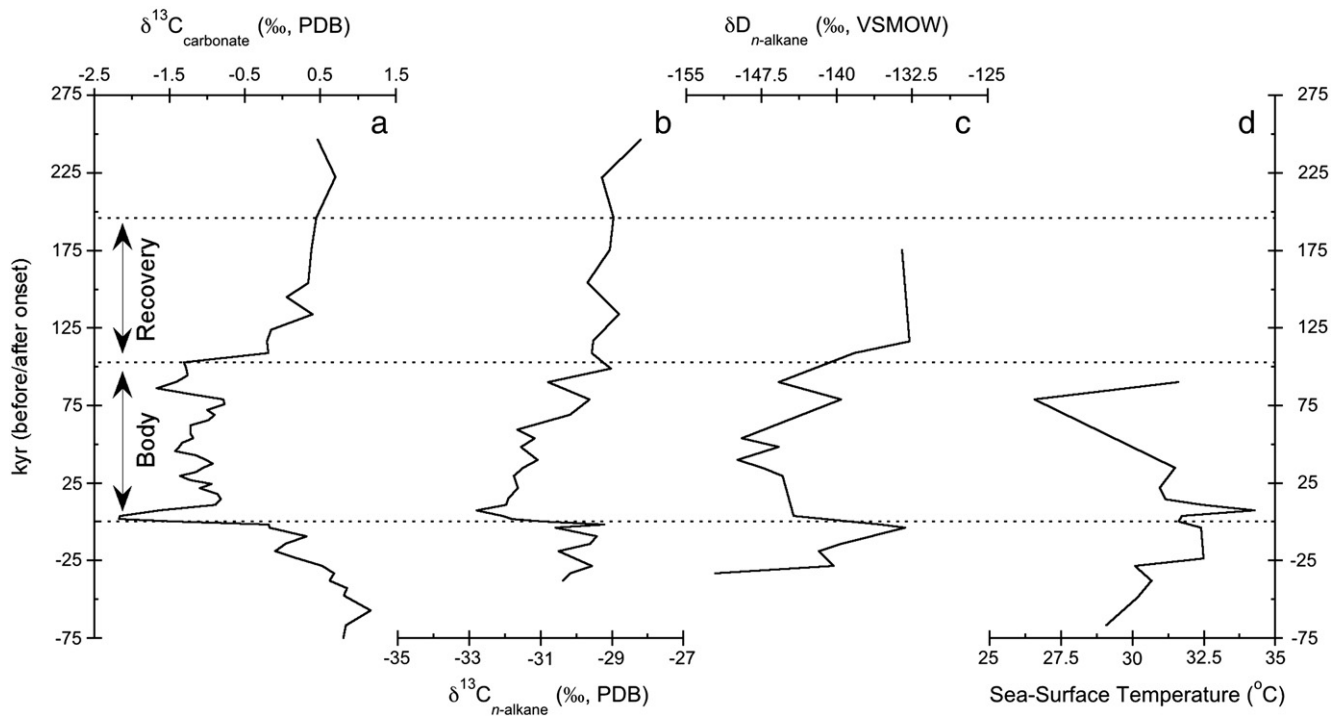


Fig. 5. Carbon isotope, hydrogen isotope, average chain length, and sea-surface temperature records from the Forada section relative to stratigraphic age. Age assignments based on Giusberti et al. (2007). Bulk carbonate $\delta^{13}\text{C}$ values (a.), $\delta^{13}\text{C}$ (b.) and δD (c.) values for $n\text{-C}_{29}$. Sea-surface temperature estimates from TEX_{86} (e.), temperature estimates from the Kim et al. (2010) calibration.

isotope values. Nonetheless, high-resolution PETM sea-surface temperature records from the Atlantic coast of North America provide some evidence for warming several thousand year prior to the onset of the CIE (Sluijs et al., 2007b). The Forada sea-surface temperature (SST) record also suggests warming of $\sim 2\text{--}3^\circ\text{C}$ prior to the onset of the CIE (Fig. 5). Similarly, pre-event warming ~ 30 kyr prior to the onset of the CIE has been interpreted from Forada planktonic foraminifera (Luciani et al., 2007), consistent with the SST records. Both planktonic foraminiferal and SST records should not be subject to the temporal offset observed in the terrestrial isotope records at Forada as they are both marine signals. Even so, Forada SST and $\delta\text{D}_{n\text{-alkane}}$ records along with records from the Arctic, and the Bighorn Basin are consistent with fundamental changes in hydrologic cycle prior to the onset of the CIE. The nature and robustness of these changes are purely speculative, but early warming (Secord et al., 2010; Sluijs et al., 2007b) or oceanographic and climatic reorganization (Thomas et al., 2002; Tripathi and Elderfield, 2004) would appear required.

5. Conclusions

High-resolution carbon and hydrogen isotope PETM records from higher-plant derived biomarkers, bulk organic carbon, and marine carbonate from the continuous and orbitally tuned Forada section in northern Italy were established to assess the marine and terrestrial expressions of the CIE and the character of warming. This work represents the first opportunity to evaluate variations between the two reservoirs at high resolution. We found differences between marine and terrestrial systems in both the temporal expressions of the CIE, as well as the magnitudes of isotope change. All Forada $\delta^{13}\text{C}$ records show a sharp spike at the onset of the PETM with the CIE determined from $\delta^{13}\text{C}_{n\text{-alkane}}$ values lagging behind the CIE expressed by both $\delta^{13}\text{C}_{\text{carbonate}}$ and $\delta^{13}\text{C}_{\text{organic}}$ values by 4–5 kyr. These results suggest the incorporation of pre-PETM n -alkanes due to soil erosion and a minimum residence time of soil n -alkanes of ~ 4000 yr during the initial phase of the CIE. In addition, we found $\delta\text{D}_{n\text{-alkane}}$ values varied prior to, and during, the PETM, consistent with a general global

pattern where mid- and high latitude sites demonstrate more negative values near the onset of the CIE. We also observe a shift to more positive $\delta\text{D}_{n\text{-alkane}}$ values prior to the onset of the CIE. These data, coupled with TEX_{86} temperature estimates, suggest both hydrologic and temperature changed prior to the onset of the CIE.

Supplementary materials related to this article can be found online at [doi:10.1016/j.epsl.2011.08.045](https://doi.org/10.1016/j.epsl.2011.08.045).

Acknowledgments

We would like to recognize three anonymous reviewers for their constructive comments, and the helpful input and discussions towards this work from S. Bohaty, H. Brinkhuis, A. Sluijs, and J. Zachos. In addition, we would like to thank N. Ceperley, K. French, and K. Metzger for their efforts in the laboratory. All isotope analyses were performed at the Yale Institute for Biospheric Studies-Earth Systems Center for Stable Isotopic Studies. This research was supported National Science Foundation Grants EAR 0628358 and OCE 0902993.

References

- Bains, S., Corfield, R.M., Norris, R.D., 1999. Mechanisms of climate warming at the end of the Paleocene. *Science* 285, 724–727.
- Bains, S., Norris, R.D., Corfield, R.M., Bowen, G.J., Gingerich, P.D., Koch, P.L., 2003. Marine-terrestrial linkages at the Paleocene–Eocene boundary. In: Wing, S.L. (Ed.), *Causes and Consequence of Globally Warm Climates in the Early Paleogene*. Geological Society of America, Denver, pp. 11–23.
- Bi, X., Sheng, G., Liu, X., Li, C., Fu, J., 2005. Molecular and carbon and hydrogen isotopic composition of n -alkanes in plant leaf waxes. *Org. Geochem.* 36, 1405–1417.
- Bol, R., Huang, Y., Meridith, J.A., Eglinton, G., Harkness, D.D., Ineson, P., 1996. The ^{14}C age and residence time of organic matter and its lipid constituents in a stagnohumic gley soil. *Eur. J. Soil Sci.* 47, 215–222.
- Bolle, M.-P., Adatte, T., 2001. Palaeocene–early Eocene climatic evolution in the Tethyan realm: clay mineral evidence. *Clay Miner.* 36, 249–261.
- Bolle, M.-P., Pardo, A., Adatte, T., Tantawy, A.A., Hinrich, K.-U., Von Salis, K., Burns, S., 2000. Climatic evolution on the southern and northern margins of the Tethys from the Paleocene to the early Eocene. *GFF* 122, 31–32.
- Bowen, G.J., Zachos, J.C., 2010. Rapid carbon sequestration at the termination of the Paleocene–Eocene Thermal Maximum. *Nat. Geosci.* 3, 866–869.
- Bowen, G.J., Koch, P.L., Gingerich, P.D., Norris, R.D., Bains, S., Corfield, R.M., 2001. Refined isotope stratigraphy across the continental Paleocene–Eocene Boundary on Polecat

- Bench in the Northern Bighorn Basin. In: Gingerich, P.D. (Ed.), *Paleocene–Eocene Stratigraphy and Biotic Change in the Bighorn and Clarks Fork Basins, Wyoming*. University of Michigan, Ann Arbor, pp. 73–88.
- Bowen, G.J., Beerling, D.J., Koch, P.L., Zachos, J.C., Quattlebaum, T., 2004. A humid climate state during the Palaeocene/Eocene thermal maximum. *Nature* 432, 495–500.
- Bralower, T.J., Thomas, D.J., Zachos, J.C., Hirschmann, M.M., Rohl, U., Sigurdsson, H., Thomas, E., Whitney, D.L., 1997. High-resolution records of the late Paleocene thermal maximum and circum-Caribbean volcanism: is there a causal link? *Geology* 25, 963–966.
- Channell, J.E.T., Medizza, F., 1981. Upper Cretaceous and Palaeogene magnetic stratigraphy and biostratigraphy from the Venetian (Southern) Alps. *Earth Planet. Sci. Lett.* 55, 419–432.
- Chikaraishi, Y., Naraoka, H., 2003. Compound-specific δD – $\delta^{13}C$ analyses of n-alkanes extracted from terrestrial and aquatic plants. *Phytochemistry* 63, 361–371.
- Clechenko, E.R., Kelly, D.C., Harrington, G.J., Stiles, C.A., 2007. Terrestrial records of a regional weathering profile at the Paleocene–Eocene boundary in the Williston Basin of North Dakota. *Geol. Soc. Am. Bull.* 119, 428–442.
- Collinson, M.E., Steart, D.C., Harrington, G.J., Hooker, J.J., Scott, A.C., Allen, L.O., Glasspool, I.J., Gibbons, S.J., 2009. Palynological evidence of vegetation dynamics in response to palaeoenvironmental change across the onset of the Paleocene–Eocene Thermal Maximum at Cobham, Southern England. *Grana* 48, 38–66.
- Collister, J., Reiley, G., Stern, B., Eglinton, G., Fry, B., 1994. Compound-specific $\delta^{13}C$ analysis of leaf lipids from plants with differing carbon dioxide metabolisms. *Org. Geochem.* 21, 619–627.
- Conte, M.H., Weber, J.C., 2002. Long-range atmospheric transport of terrestrial biomarkers to the western North Atlantic. *Glob. Biogeochem. Cycles* 16, 1142.
- Cramer, B.S., Aubry, M.-P., Miller, K.G., Olsson, R.K., Wright, J.D., Kent, D.V., 1999. An exceptional chronologic, isotopic, and clay mineralogical record of the latest Paleocene thermal maximum, Bass River, NJ, ODP 174AX. *Bull. Soc. Geol. Fr.* 170, 883–897.
- Cramer, B.S., Wright, J.D., Kent, D.V., Aubry, M.-P., 2003. Orbital climate forcing of $\delta^{13}C$ excursions in the late Paleocene–early Eocene (chrons C24n–C25n). *Paleoceanography* 18, 1097.
- Crouch, E.M., Visscher, H., 2003. Terrestrial vegetation record across the initial Eocene thermal maximum at the Tawanui marine section, New Zealand. *Geol. Soc. Am. Spec. Pap.* 369, 351–363.
- Crouch, E.M., Dickens, G.R., Brinkhuis, H., Aubry, M.-P., Hollis, C.J., Rogers, K.M., Visscher, H., 2003. The Apectodinium acme and terrestrial discharge during the Paleocene–Eocene thermal maximum: new palynological, geochemical and calcareous nannoplankton observations at Tawanui, New Zealand. *Palaeogeogr. Palaeoclimatol. Palaeoecol.* 194, 387–403.
- Cui, Y., Kump, L.R., Ridgwell, A.J., Charles, A.J., Junium, C.K., Diefendorf, A.F., Freeman, K.H., Urban, N.M., Harding, I.C., 2011. Slow Release of Fossil Carbon During the Paleocene–Eocene Thermal Maximum. *Nat. Geosci.* 4, 481–485.
- Dickens, G.R., O’Neil, J.R., Rea, D.K., Owen, R.M., 1995. Dissociation of oceanic methane hydrate as a cause of the carbon isotope excursion at the end of the Paleocene. *Paleoceanography* 10, 965–971.
- Dickens, G.R., Castillo, M.M., Walker, J.C.G., 1997. A blast of gas in the latest Paleocene: simulating first-order effects of massive dissociation of oceanic methane hydrate. *Geology* 25, 259–262.
- Diefendorf, A.F., Mueller, K.E., Wing, S.L., Koch, P.L., Freeman, K.H., 2010. Global patterns in leaf ^{13}C discrimination and implications for studies of past and future climate. *Proc. Natl. Acad. Sci.* 107, 5738–5743.
- Drenzek, N.J., Montlucon, D.B., Yunker, M.B., Macdonald, R.W., Eglinton, T.J., 2007. Constraints on the origin of sedimentary organic carbon in the Beaufort Sea from coupled molecular ^{13}C and ^{14}C measurements. *Mar. Chem.* 103, 146–162.
- Eglinton, G., Hamilton, R.J., 1967. Leaf epicuticular waxes. *Science* 156, 1322–1335.
- Eglinton, T.L., Benitez-Nelson, B., Pearson, A., McNichol, A.P., Bauer, J.E., Druffel, E.R.M., 1997. Variability in radiocarbon ages of individual organic compounds from marine sediments. *Science* 277, 796–799.
- Eldholm, O., Thomas, E., 1993. Environmental impact of volcanic margin formation. *Earth Planet. Sci. Lett.* 117, 319–329.
- Gibson, T.G., Bybell, L.M., Mason, D.B., 2000. Stratigraphic and climatic implications of clay mineral changes around the Paleocene/Eocene boundary of the northeastern US margin. *Sediment. Geol.* 134, 65–92.
- Giusberti, L., Rio, D., Agnini, C., Backman, J., Fornaciari, E., Tateo, F., Oddone, M., 2007. Mode and tempo of the Paleocene–Eocene thermal maximum in an expanded section from the Venetian pre-Alps. *Geol. Soc. Am. Bull.* 119, 391–412.
- Greenwood, D.R., Wing, S.L., 1995. Eocene continental climates and latitudinal temperature gradients. *Geology* 23, 1044–1048.
- Handley, L., Pearson, P.N., McMillan, I.K., Pancost, R.D., 2008. Large terrestrial and marine carbon and hydrogen isotope excursions in a new Paleocene/Eocene boundary section from Tanzania. *Earth Planet. Sci. Lett.* 275, 17–25.
- Hasegawa, T., Yamamoto, S., Pratt, L.M., 2006. Data report: stable carbon isotope fluctuation of longchain n-alkanes from Leg 208 Hole 1263A across the Paleocene/Eocene boundary. In: Kroon, D., Zachos, J.C., Richter, C. (Eds.), *Proceedings of the Ocean Drilling Program, Scientific Results*. Ocean Drilling Program, College Station, TX, pp. 1–11.
- Higgins, J.A., Schrag, D.P., 2006. Beyond methane: towards a theory for the Paleocene–Eocene Thermal Maximum. *Earth Planet. Sci. Lett.* 245, 523–537.
- Hopmans, E.C., Weijers, J.W.H., Schefuss, E., Herfort, L., Sinninghe Damste, J.S., Schouten, S., 2004. A novel proxy for terrestrial organic matter in sediments based on branched and isoprenoid tetraether lipids. *Earth Planet. Sci. Lett.* 224, 107–116.
- Hou, J., Huang, Y., Oswald, W.W., Foster, D.R., Shuman, B., 2007. Centennial-scale compound-specific hydrogen isotope record of Pleistocene–Holocene climate transition from southern New England. *Geophys. Res. Lett.* 34, L19706.
- Huang, Y., Li, B., Bryant, C., Bol, R., Eglinton, G., 1999. Radiocarbon dating of aliphatic hydrocarbons: A new approach for dating passive-fraction carbon in soil horizons. *Soil Sci. Soc. Am. J.* 63, 1181–1187.
- Huber, M., Sloan, L.C., 1999. Warm climate transitions: a general circulation modeling study of the Late Paleocene Thermal Maximum (56 Ma). *J. Geophys. Res.* 104, 16633–16655.
- Jaramillo, C., Ochoa, D., Contreras, L., Pagani, M., Carvajal-Ortiz, H., Pratt, L.M., Krishnan, S., Cradonna, A., Romero, M., Quiroz, L., Rodriguez, G., Rueda, M.J., de la Parra, F., Moron, S., Green, W., Bayona, G., Montes, C., Quintero, O., Ramirez, R., Mora, G., Schouten, S., Bermudez, H., Navarrete, R., Parra, F., Alvaran, M., Osorno, J., Crowley, J.L., Valencia, V., Verwoort, J., 2010. Effects of rapid global warming at the Paleocene–Eocene boundary on neotropical vegetation. *Science* 330, 957–961.
- Johns, C.M., Bohaty, S.M., Zachos, J.C., Slujs, A., Gibbs, S., Brinkhuis, H., Bralower, T.J., 2008. North American continental margin records of the Paleocene–Eocene thermal maximum: implications for global carbon and hydrological cycling. *Paleoceanography* 23, PA2217.
- Kaiho, K., Arinobu, T., Ishiwatari, R., Morgans, H.E.G., Okada, H., Takeda, N., Takaki, K., Zhou, G., Kajiwara, Y., Matsumoto, R., Hirai, A., Niitsuma, N., Wada, H., 1996. Latest Paleocene benthic foraminiferal extinction and environmental changes at Tawanui, New Zealand. *Paleoceanography* 11, 447–465.
- Kennett, J.P., Stott, L.D., 1991. Abrupt deep-sea warming, palaeoceanographic changes and benthic extinctions at the end of the Paleocene. *Nature* 353, 225–229.
- Kim, J.-H., van der Meer, J., Schouten, S., Helmke, P., Willmott, V., Sanglorgi, F., Koc, N., Hopmans, E.C., Sinninghe Damste, J.S., 2010. New indices and calibrations derived from the distribution of crenarchaeal isoprenoid tetraether lipids: Implications for past sea surface temperature reconstructions. *Geochim. Cosmochim. Acta* 74, 4639–4654.
- Koch, P.L., Zachos, J.C., Dettman, D.L., 1995. Stable isotope stratigraphy and paleoclimatology of the Paleocene Bighorn Basin (Wyoming, USA). *Palaeogeogr. Palaeoclimatol. Palaeoecol.* 115, 61–89.
- Kopp, R.E., Schumann, D., Raub, T.D., Powars, D.S., Godfrey, L.V., Swanson-Hysell, N.L., Maloof, A.C., Vali, H., 2009. An Appalachian Amazon? Magnetofossil evidence for the development of a tropical river-like system in the mid-Atlantic United States during the Paleocene–Eocene thermal maximum. *Paleoceanography* 24.
- Kurtz, A.C., Kump, L.R., Arthur, M.A., Zachos, J.C., Paytan, A., 2003. Early Cenozoic decoupling of the global carbon and sulfur cycles. *Paleoceanography* 18, 1090.
- Luciani, V., Giusberti, L., Agnini, C., Backman, J., Fornaciari, E., Rio, D., 2007. The Paleocene–Eocene thermal maximum as recorded by tethyan planktonic foraminifera in the forada section (northern Italy). *Mar. Micropaleontol.* 64, 189–214.
- Magioncalda, R., Dupuis, C., Smith, T., Steurbaut, E., Gingerich, P.D., 2004. Paleocene–Eocene carbon isotope excursion in organic carbon and pedogenic carbonate: direct comparison in a continental stratigraphic section. *Geology* 32, 553–556.
- McCarren, H.K., Thomas, E., Hasegawa, T., Rohl, U., Zachos, J.C., 2008. Depth dependency of the Paleocene–Eocene carbon isotope excursion: Paired benthic and terrestrial biomarker records (Ocean Drilling Program Leg 208, Walvis Ridge). *Geochim. Geophys. Geosyst.* 9.
- McInerney, F.A., Wing, S.L., 2011. The Paleocene–Eocene Thermal Maximum: A perturbation of carbon cycle, climate and biosphere with implications for the future. *Annu. Rev. Earth Planet. Sci.* 39, 489–516.
- Meyers, P.A., 1994. Preservation of elemental and isotopic source identification of sedimentary organic matter. *Chem. Geol.* 114, 289–302.
- Murphy, B.H., Farley, K.A., Zachos, J.C., 2010. An extraterrestrial 3He -based timescale for the Paleocene–Eocene thermal maximum (PETM) from Walvis Ridge, IODP Site 1266. *Geochim. Cosmochim. Acta* 74, 5098–5108.
- Pagani, M., Pedentchouk, N., Huber, M., Slujs, A., Schouten, S., Brinkhuis, H., Sinninghe Damste, J.S., Dickens, G.R., the Expedition 302 Scientists, 2006. Arctic hydrology during global warming at the Paleocene/Eocene thermal maximum. *Nature* 442, 671–675.
- Paul, E.A., Follett, R.F., Leavitt, S.W., Halvorson, A., Peterson, G.A., Lyon, D.J., 1997. Radiocarbon dating for determination of soil organic matter pool sizes and dynamics. *Soil Sci. Soc. Am. J.* 61, 1058–1067.
- Pedentchouk, N., Sumner, W., Tipple, B.J., Pagani, M., 2008. $\delta^{13}C$ and δD compositions of n-alkanes from modern angiosperms and conifers: an experimental set up in central Washington State, USA. *Org. Geochem.* 39, 1066–1071.
- Peters, K.E., Walters, C.C., Moldovan, J.M., 2005. *The Biomarker Guide: II Biomarkers and Isotopes in Petroleum Systems and Earth History*, 2nd edition. Cambridge University Press, Cambridge.
- Pierrehumbert, R.T., 2002. The hydrologic cycle in deep-time climate problems. *Nature* 419, 191–198.
- Raymond, P.A., Bauer, J.E., 2001. Riverine export of aged terrestrial organic matter to the North Atlantic Ocean. *Nature* 409, 497–500.
- Robert, C., Chamley, H., 1991. Development of early Eocene warm climates, as inferred from clay mineral variations in oceanic sediments. *Palaeogeogr. Palaeoclimatol. Palaeoecol.* 89, 315–331.
- Robert, C., Kennett, J.P., 1994. Antarctic subtropical humid episode at the Paleocene–Eocene boundary: clay-mineral evidence. *Geology* 22, 211–214.
- Roden, J.S., Lin, G., Ehleringer, J.R., 2000. A mechanistic model for interpretation of hydrogen and oxygen isotope ratios in tree-ring cellulose. *Geochim. Cosmochim. Acta* 64, 21–35.
- Rohl, U., Bralower, T.J., Norris, R.D., Wefer, G., 2000. New chronology for the late Paleocene thermal maximum and its environmental implications. *Geology* 28, 927–930.
- Rohl, U., Westerhold, T., Bralower, T.J., Zachos, J.C., 2007. On the duration of the Paleocene–Eocene thermal maximum. *Geochim. Geophys. Geosyst.* 8, Q12002.
- Sachse, D., Radke, J., Gleixner, G., 2006. δD values of individual n-alkanes from terrestrial plants along a climatic gradient—implications for the sedimentary biomarker record. *Org. Geochem.* 37, 469–483.
- Sachse, D., Kahmen, A., Gleixner, G., 2009. Significant seasonal variation in the hydrogen isotopic composition of leaf-wax lipids for two deciduous tree ecosystems (*Fagus sylvatica* and *Acer pseudoplatanus*). *Org. Geochem.* 40, 732–742.
- Schmitz, B., Pujalte, V., 2003. Sea-level, humidity, and land-erosion records across the initial Eocene thermal maximum from a continental-marine transect in northern Spain. *Geology* 31, 689–692.

- Schmitz, B., Pujalte, V., 2007. Abrupt increase in seasonal extreme precipitation at the Paleocene–Eocene boundary. *Geology* 35, 215–218.
- Schouten, S., Woltering, M., Rijpstra, W.I.C., Sluijs, A., Brinkhuis, H., Sinninghe Damste, J.S., 2007. The Paleocene–Eocene carbon isotope excursion in higher plant organic matter: differential fractionation of angiosperms and conifers in the Arctic. *Earth Planet. Sci. Lett.* 258, 581–592.
- Secord, R., Gingerich, P.D., Lohmann, K.C., MacLeod, K.G., 2010. Continental warming preceding the Palaeocene–Eocene thermal maximum. *Nature* 467, 955–958.
- Shellito, C.J., Sloan, L.C., Huber, M., 2003. Climate model sensitivity to atmospheric CO₂ levels in the Early–Middle Paleogene. *Palaeogeogr. Palaeoclimatol. Palaeoecol.* 193, 113–123.
- Sluijs, A., Schouten, S., Pagani, M., Woltering, M., Brinkhuis, H., Sinninghe Damste, J.S., Dickens, G.R., Huber, M., Reichart, G.-J., Stein, R., Matthiessen, J., Lourens, L.J., Pedentchouk, N., Backman, J., Moran, K., t. E. Scientists, 2006. Subtropical Arctic Ocean temperatures during the Palaeocene/Eocene thermal maximum. *Nature* 441, 610–613.
- Sluijs, A., Brinkhuis, H., Schouten, S., Bohaty, S., John, C.M., Zachos, J.C., Reichart, G.-J., Sinninghe Damste, J.S., Crouch, E.M., Dickens, G.R., 2007a. Environmental precursors to rapid light carbon injection at the Palaeocene/Eocene boundary. *Nature* 450, 1218–1221.
- Sluijs, A., Bowen, G.J., Brinkhuis, H., Lourens, L.J., Thomas, E., 2007b. The Palaeocene–Eocene Thermal Maximum super greenhouse: biotic and geochemical signatures, age models and mechanisms of global change. In: Williams, M., Haywood, A.M., Gregory, F.J., Schmidt, D.N. (Eds.), *Geological Society Special Publication*, pp. 323–349.
- Smith, F.A., Freeman, K.H., 2006. Influence of physiology and climate on δD of leaf wax *n*-alkanes from C3 and C4 grasses. *Geochim. Cosmochim. Acta* 70, 1172–1187.
- Smith, F.A., Wing, S.L., Freeman, K.H., 2007. Magnitude of the carbon isotope excursion at the Paleocene–Eocene thermal maximum: the role of plant community change. *Earth Planet. Sci. Lett.* 262, 50–65.
- Smittenberg, R.H., Hoppmans, E.C., Schouten, S., Hayes, J.M., Eglinton, T.I., Sinninghe Damste, J.S., 2004. Compound-specific radiocarbon dating of the varved Holocene sedimentary record of Saanich Inlet, Canada. *Paleoceanography* 19, PA2012.
- Stoll, H.M., 2005. Limited range of interspecific vital effects in coccolith stable isotopic records during the Paleocene–Eocene thermal maximum. *Paleoceanography* 20.
- Svensen, H., Planke, S., Mørner, A., Jamveit, B., Myklebust, R., Eidem, T.R., Rey, S.S., 2004. Release of methane from a volcanic basin as a mechanism for initial Eocene global warming. *Nature* 429, 542–545.
- Thomas, D.J., Bralower, T.J., Zachos, J.C., 1999. New evidence for subtropical warming during the late Paleocene thermal maximum: stable isotopes from Deep Sea Drilling Project Site 527, Walvis Ridge. *Paleoceanography* 14, 561–570.
- Thomas, D.J., Zachos, J.C., Bralower, T.J., Thomas, E., Bohaty, S.M., 2002. Warming the fuel for the fire: evidence for the thermal dissociation of methane hydrate during the Paleocene–Eocene thermal maximum. *Geology* 30, 1067–1070.
- Tripati, A.K., Elderfield, H., 2004. Abrupt hydrographic changes in the equatorial Pacific and subtropical Atlantic from foraminiferal Mg/Ca indicate greenhouse origin for the thermal maximum at the Paleocene–Eocene Boundary. *Geochim. Geophys. Geosyst.* 5, Q02006.
- Utescher, T., Mosbrugger, V., 2007. Eocene vegetation patterns reconstructed from plant diversity—a global perspective. *Palaeogeogr. Palaeoclimatol. Palaeoecol.* 247, 243–271.
- Wakeham, S.G., Pease, T.K., 1992. *Lipid Analysis in Marine Particles and Sediment Samples*. Skidaway Institute of Oceanography, Savannah, GA.
- Weijers, J.W.H., Schouten, S., Sluijs, A., Brinkhuis, H., Sinninghe Damste, J.S., 2007. Warm arctic continents during the Palaeocene–Eocene thermal maximum. *Earth Planet. Sci. Lett.* 261, 230–238.
- White, P.D., Schiebout, J., 2008. Paleogene paleosols and changes in pedogenesis during the initial Eocene thermal maximum: Big Bend National Park, Texas, USA. *Geol. Soc. Am. Bull.* 120, 1347–1361.
- Wilf, P., 2000. Late Paleocene–early Eocene climate changes in southwestern Wyoming: Paleobotanical analysis. *Geol. Soc. Am. Bull.* 112, 292–307.
- Wing, S.L., Harrington, G.J., 2001. Floral response to rapid warming in the earliest Eocene and implications for concurrent faunal change. *Paleobiology* 27, 539–563.
- Wing, S.L., Harrington, G.J., Smith, F.A., Bloch, J.J., Boyer, D.M., Freeman, K.H., 2005. Transient floral change and rapid global warming at the Paleocene–Eocene Boundary. *Science* 310, 993–996.
- Zachos, J.C., Pagani, M., Sloan, L., Thomas, E., Billups, K., 2001. Trends, rhythms, and aberrations in global climate 65 Ma to present. *Science* 292, 686–693.
- Zachos, J.C., Wara, M.W., Bohaty, S.M., Delaney, M.L., Petrizzo, M.R., Brill, A., Bralower, T.J., Premoli-Silva, I., 2003. A transient rise in tropical sea surface temperature during the Paleocene–Eocene Thermal Maximum. *Science* 302, 1551–1554.
- Zachos, J.C., Rohl, U., Schellenberg, S.A., Sluijs, A., Hodell, D.A., Kelly, D.C., Thomas, E., Nicolo, M., Raffi, I., Lourens, L.J., McCarrren, H.K., Kroon, D., 2005. Rapid acidification of the ocean during the Paleocene–Eocene Thermal Maximum. *Science* 308, 1611–1615.
- Zachos, J.C., Schouten, S., Bohaty, S., Quattlebaum, T., Sluijs, A., Brinkhuis, H., Gibbs, S., Bralower, T.J., 2006. Extreme warming of mid-latitude coastal ocean during the Paleocene–Eocene Thermal Maximum: inferences from TEX86 and isotope data. *Geology* 34, 737–740.
- Zeebe, R.E., Zachos, J.C., Dickens, G.R., 2009. Carbon dioxide forcing alone insufficient to explain Palaeocene–Eocene Thermal Maximum warming. *Nat. Geosci.* 2, 576–580.
- Zhou, Y., Grice, K., Stuart-Williams, H., Farquhar, G.D., Hocart, C.H., Lu, H., Liu, W., 2010. Biosynthetic origin of the saw-toothed profile in $\delta^{13}C$ and δ^2H of *n*-alkanes and systematic isotopic differences between *n*-, iso- and anteiso-alkanes in leaf waxes of land plants. *Phytochemistry* 71, 388–403.